Field-induced phase transitions in an antiferroelectric liquid crystal using the pyroelectric effect

N. M. Shtykov,[1,2] J. K. Vij,[1,*] R. A. Lewis,[3] M. Hird,[3] and J. W. Goodby[3]
[1]*Department of Electronic and Electrical Engineering, Trinity College, University of Dublin, Dublin 2, Ireland*
[2]*Institute of Crystallography, Russian Academy of Sciences, Leninskii Prospekt 59, 117333 Moscow, Russia*
[3]*Department of Chemistry, University of Hull, Cottingham Road, Hull HU6 7RX, United Kingdom*
(Received 23 July 1999)

The antiferroelectric liquid crystal (AFLC) under investigation possesses different helical polar phases. Measurements of pyroelectric response of these phases as a function of temperature and bias field have elucidated the ability of this method for investigating the nature of antiferroelectric phases and phase transitions under the bias field. The pyroelectric signal as a function of the bias field at fixed temperatures and as a function of temperature for fixed bias fields was measured for different phases of the investigated AFLC material. A theoretical model describing the pyroelectric response in different phases of AFLC is given, and the experimental results are interpreted. The threshold fields for field induced phase transitions are determined. The type of field induced phase transition from the AF phase in particular is found to be dependent on the temperature within its range. The properties of an unusual ferrielectric phase existing between ferrielectric chiral smectic-*C* (Sm*C**) and antiferroelectric AF phases are studied in a great detail. The results confirm that this phase is one of the incommensurate phases, predicted by the axial next-nearest neighbor Ising model and Landau model for this temperature region.

PACS number(s): 42.70.Df, 61.30.−v, 64.70.Md

I. INTRODUCTION

Antiferroelectric liquid crystals (AFLC's) exhibit several chiral phases between paraelectric smectic *A* (Sm*A**) and antiferroelectric smectic C_A (SmC_A^*). These phases were tentatively designated as SmC_α^*, SmC_β^*, and SmC_γ^* in order of decreasing temperature [1]. Among these phases SmC_α^* seems to be more complicated than the other phases. Finally, this series of phases was added by the discovery of a number of additional ferrielectric and antiferroelectric phases. The existence of some of the ferrielectric phases is very sensitive to the optical purity of the AFLC's. It was reported that phases SmC_α^* and SmC_γ^*, which have ferrielectric properties, disappear with decreasing optical purity [2]. The SmC_β^* phase is usually considered to be the same as the ferroelectric chiral smectic *C* (Sm*C**). But some researchers believe that the SmC_β^* phase in optically pure samples should be considered as ferrielectric and not ferroelectric. It was also confirmed that a decrease in the optical purity causes the phase transition SmC_β^* to Sm*C** phase [3]. X-ray resonant technique employed on a thiobenzoate liquid-crystal compound has recently shown [4] the existence of four phases with different superlattice periodicities. These phases are SmC_A^*, SmC_{FI1}^*, and SmC_{FI2}^*, with two-, three-, and four-layer superlattices, respectively, and SmC_α^*, with a periodicity incommensurate with the layer spacing. In the SmC_α^* phase an incommensurate periodicity was shown to lie roughly between from eight and five layers with decreasing temperature.

The appearance of antiferroelectric and ferrielectric phases in the tilted chiral smectic liquid crystals can be understood to be a result of the competition between the antiferroelectric and ferroelectric interactions in adjacent smectic layers. This competition produces different periodic (*A* + *F*) sequences of antiferroelectric (*A*) and ferroelectric (*F*) orderings among the smectic layers. Several different theoretical approaches have been advanced for explaining a variety of the ferrielectric phases, and these postulates are based mostly at the expanded Landau model [5–7] or on the one-dimensional Ising model [8] and the axial next-nearest-neighbor Ising (ANNNI) model [9–12]. Recently, the short pitch modes model [13] was presented, which describes antiferroelectric and ferrielectric phases as structures with certain 'families' of modulation modes.

We take the ANNNI model, advanced for the antiferroelectric and ferrielectric phases in an electric field [12], as the basis for explaining a variety of different phase transitions observed in our pyroelectric experiments. The Hamiltonian of the system with the third-nearest-neighbor interaction in the electric field *E* is given by

$$H = -J\sum_{(i,j)} s_i s_j - J_1\sum_i^A s_i s_{i+1} - J_2\sum_i^A s_i s_{i+2} - J_3\sum_i^A s_i s_{i+3} - E\sum_i s_i, \quad (1)$$

where the molecular state is expressed in terms of the Ising spin ($s_i = \pm 1$), designating the direction of the molecular tilt, J, J_1, J_2, and J_3 the interaction parameters, the first summation is taken over the nearest-neighbor pairs of molecules in the same smectic layer and the second, third, and fourth ones are over those between the first-, second-, and third-nearest-neighbor layers, respectively. The superscript *A* denotes the axial direction. An essential and characteristic point of this model is the negative value for the energy parameter J_2.

*Corresponding author. Email address: jvij@tcd.ie

In mean field theory, the thermodynamical potential is obtained as

$$\Phi_p=\frac{1}{p}\sum_{i=1}^{p}\left(-\frac{Jz}{2}\sigma_i^2-J_1\sigma_i\sigma_{i+1}-J_2\sigma_i\sigma_{i+2}-J_3\sigma_i\sigma_{i+3}\right.$$
$$\left.-E\sigma_i+\frac{T}{2}\{(1+\sigma_i)\ln(1+\sigma_i)+(1-\sigma_i)\ln(1-\sigma_i)\}\right), \tag{2}$$

where the order parameter σ_i is the thermal average of s_i, p denotes the period of the ordered structure ($\sigma_{i\pm p}=\sigma_i$), T the absolute temperature (a unit system was chosen with the Boltzmann constant equal to unity), and z the coordination number in the layer. The equilibrium conditions

$$-Jz\sigma_i-J_1(\sigma_{i-1}+\sigma_{i+1})-J_2(\sigma_{i-2}+\sigma_{i+2})$$
$$-J_3(\sigma_{i-3}+\sigma_{i+3})-E+\frac{T}{2}\ln\frac{1+\sigma_i}{1-\sigma_i}=0$$
$$(i=1,2,...,p), \tag{3}$$

derived by minimizing Eq. (2) with respect to σ_i, are solved numerically to obtain the phase diagram of the system in the electric field (Fig. 1 from Ref. [12]). In some cases, the jumps of the order parameters at the transition points from the modulated phases to the uniform one are small. In order to study the instability of the uniform phase, the order parameter σ_i is $\sigma_i=\sigma_0+u_i$, where σ_0, the value of σ_i at the uniform phase, is determined from the equilibrium condition

$$(-Jz-2J_1-2J_2-2J_3)\sigma_0-E+\frac{T}{2}\ln\frac{1+\sigma_0}{1-\sigma_0}=0. \tag{4}$$

Then the thermodynamical potential is expressed as

$$\Phi=\Phi(\sigma_0)+\frac{1}{2}\sum_q F_q|u(q)|^2+O(u^3), \tag{5}$$

in which $u(q)$ denotes the Fourier transforms of the deviation u_i, and F_q is given by

$$F_q=-Jz+\frac{T}{1-\sigma_0^2}$$
$$-2(J_1\cos 2\pi q+J_2\cos 4\pi q+J_3\cos 6\pi q). \tag{6}$$

Instability of the uniform phase with respect to periodic perturbation occurs when the minimum eigenvalue vanishes, that is, $F_q=0$, where the corresponding wave number q is determined from

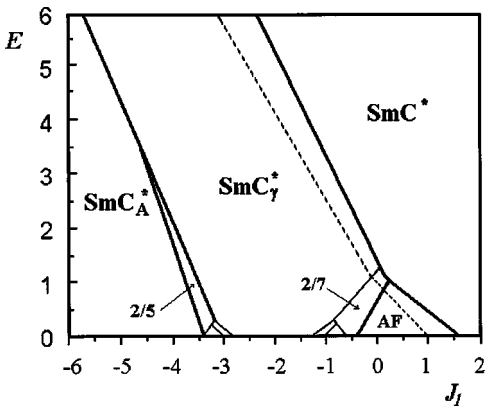

FIG. 1. Phase diagram on E vs J_1 plane for normalized $T=6.0$. Two subphases are indicated by their wave numbers. The solid lines show the coexisting curves, and the broken line shows the instability curve given by $F_q=0$.

$$J_1\sin 2\pi q+2J_2\sin 4\pi q+3J_3\sin 6\pi q=0. \tag{7}$$

This model predicts all the main phases observed in AFLC's, SmC^* ($q=0$), SmC_A^* ($q=\frac{1}{2}$), SmC_γ^* ($q=\frac{1}{3}$), and AF ($q=\frac{1}{4}$). q is the reciprocal of the layer period (number of layers in a periodic structure). In addition to the existence of main phases, it also predicts a series of incommensurate subphases designated by the wave numbers $\frac{2}{5}$, $\frac{3}{8}$, $\frac{4}{11}$, $\frac{2}{7}$, $\frac{3}{10}$, and $\frac{4}{13}$; two of them, $\frac{2}{5}$ and $\frac{2}{7}$, with the largest regions of existence, are shown in Fig. 1. The phase diagram was calculated for a normalized temperature $T=6.0$; the energy parameters are scaled in the unit $|J_2|$, and values $Jz=6$ and $J_3=0.3$ are utilized. The broken curve shows the instability line of the uniform phase SmC^*.

We use a method developed earlier [14] for pyroelectric measurements of FLC's and AFLC's under the action of external electric field. The pyroelectric signal as a function of bias field at fixed temperatures and as a function of temperature at fixed bias fields was obtained for different phases of the AFLC material. Dielectric measurements and macroscopic polarization observations were also carried out to complement the pyroelectric results. We also present a theoretical model for the origin of the pyroelectric effect in different phases of AFLC's for explaining the experimental results.

II. EXPERIMENT

The AFLC material used in our experiments was synthesized in Hull is (R)-(-)-1-methylheptyl 4-(4′-dodecyloxybiphenyl-4-ylcarbonyloxy)-3-fluorobenzoate, with acronym 12OF1M7. The molecular structure is given as

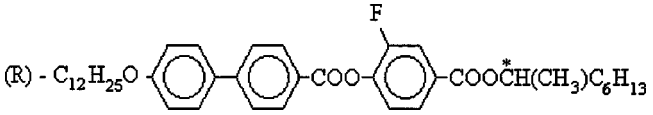

The following phase transition sequence for this material has been found under cooling, using conoscopy and the spontaneous polarization measurements [15,16]

$\mathrm{Sm}C_A^*$ (78 °C) $\mathrm{Sm}C_\gamma^*$ (81 °C) AF (83 °C) FiLC (90 °C) SmC^* (93 °C) SmA^*(106 °C) Isotropic.

Here AF denotes the antiferroelectric phase, with a structure different than the $\mathrm{Sm}C_A^*$ phase. This phase corresponds to the layer structure of $\mathrm{Sm}C_{FI2}^*$ given by Mach *et al.* [4]. The ferrielectric liquid crystal (FiLC) phase exists over a wide range of temperatures with characteristics different from those of the SmC^* phase. In our previous paper [17], we reported that in the optically pure samples of this material, the $\mathrm{Sm}C_\alpha^*$ phase can exist in the temperature range from 94.4 °C to 93 °C.

A cell of 15-μm sample thickness, used for dielectric and pyroelectric measurements, consisted of two glass plates with a indium tin oxide (ITO) layers as electrodes and the Mylar thin-film stripes as spacers. The dimensions of the working area of the electrodes was $4.5\times4.5\,\mathrm{mm}^2$. Polyimide films (Nissan Chemical Industry, RN-1266) were coated on the ITO electrodes, cured for a duration of 1 h at a temperature of 250 °C, and then rubbed in one direction using a velvet track to achieve the alignment. The cell was heated and filled with the antiferroelectric compound in the isotropic phase, and cooled slowly to the SmA^* phase.

For investigating the macroscopic polarization in different phases of the AFLC material, we used the pyroelectric method given in Ref. [14]. The temperature measurements were carried out during continuous cooling at a rate of 0.1 °C/min. The dependencies of the pyroelectric response on the bias field were measured at stabilized temperatures at the rate of voltage increase of 0.3 V/min. Dielectric measurements at a frequency of 1 kHz with application of bias field were made using an HP-4192A impedance analyzer.

III. THEORETICAL MODEL OF PYROELECTRICS IN AFLC PHASES

Pyroelectricity is a fundamental property of materials which have a spontaneous polarization, such as ferroelectrics, ferrielectrics, and antiferroelectrics, and is due to a change in the spontaneous polarization with temperature. Glass *et al.* [18] were the first to use the Chynoweth technique [19] for investigating the pyroelectric properties of ferroelectric liquid crystals. This technique involves the dynamic heating of a sample with a chopped laser beam, and the detection of the pyroelectric signal using a lock-in amplifier. Beresnev and Blinov [20] used a pulsed Nd-glass laser for measuring the temperature dependence of the spontaneous polarization, for the electric field dependence of the pyroelectric coefficient, and for observing the phase transitions.

In our pyroelectric experiments, the AFLC cell is irradiated by white light from a halogen lamp whose intensity is modulated at a frequency of 125 Hz with a chopper. Light absorption by the ITO electrodes and in turn by the AFLC's, leads to the modulation of the sample temperature at the same frequency.

The pyroelectric signal generation may be described in terms of the time-dependent electric displacement $\mathbf{D}(\mathbf{r},t)$ which arises from the modulation of the temperature $T(\mathbf{r},t)$ of the sample. Here $\mathbf{r}$ is a spatial coordinate vector, and t is time. The electric displacement, along the bias electric field direction, i.e., the X axis, is given by $D(\mathbf{r},t)=\varepsilon_0\varepsilon(\mathbf{r},t)E_{\mathrm{dc}}+P(\mathbf{r},t)$; $\varepsilon_0=8.85\times10^{-12}$ F/m is the permittivity of free space, $\varepsilon(\mathbf{r},t)$ is the relative permittivity of the liquid crystal, E_{dc} is the bias electric field, and $P(\mathbf{r},t)$ is a projection of the spontaneous polarization of the liquid crystal on the X axis. We assume that all quantities vary only in the direction of the helix axis (i.e., the Z axis) and are constant in both X and Y axes. The current density $j(z,t)$, at location z and time t, is given by the derivative of the electric displacement $D(z,t)$ on t. The total pyroelectric current $J(t)$ is proportional to the value of the current density $j(z,t)$, averaged over the helical pitch Z, and the area of the sample electrode A,

$$J(t)=\frac{A}{Z}\int_0^z\frac{\partial D(z,t)}{\partial t}dz=A\left(\varepsilon_0\frac{d\overline{\varepsilon}}{dt}E_{\mathrm{dc}}+\frac{d\overline{P}}{dt}\right), \tag{8}$$

where $\overline{\varepsilon}$ and $\overline{P}$ denote averaged values of permittivity and polarization over the z coordinate. The time dependence of the relative permittivity and polarization is caused by the time dependence of the temperature. Therefore, we can rewrite Eq. (8) in another form:

$$\begin{aligned}J(t)&=A\left(\varepsilon_0\frac{d\overline{\varepsilon}}{dT}E_{\mathrm{dc}}+\frac{d\overline{P}}{dT}\right)\frac{dT}{dt}\\&=A\left(\varepsilon_0\frac{d\overline{\varepsilon}}{dT}E_{\mathrm{dc}}+\gamma\right)\frac{dT}{dt}=A\gamma_T\frac{dT}{dt}.\end{aligned} \tag{9}$$

γ_T denotes the sum of the intrinsic pyroelectric coefficient $\gamma=dP/dT$ due to the spontaneous polarization and the contribution induced by the external electric field. The pyroelectric voltage V_{pyr} measured by a lock-in amplifier at the frequency of light modulation (125 Hz) is proportional to the pyroelectric current, and hence to the pyroelectric coefficient γ_T.

In a one-dimensional Ising model [8], phases of an AFLC are specified by the irreducible rational parameter $q_T=F/(F+A)=m/n$, which means the fraction of ferroelectric orderings (F) in the periodic structure $(F+A)$, where m and n are integer numbers. The phases which have either m or n even possess zero spontaneous polarization, and are considered as antiferroelectric phases. In the ferrielectric phases both m and n are odd, and the spontaneous polarization is equal to P_S/n, where P_S is a spontaneous polarization of ferroelectric SmC^* phase. Therefore, in terms of this model for a zero external field we can represent the spontaneous polarization of the ith phase as $P_i=r_iP_S$, where r_i is a coefficient depending on the phase structure. In antiferroelectric phases $r_i=0$, in the ferroelectric SmC^* phase $r_i=1$ $(=1/n,n=1)$, and in ferrielectric phases with the parameters $q_T=m/n$, $r_i=1/n$. The wave number q, which is used for phase characterization in the ANNNI model, is related to q_T in Refs. [1], [8] by $q=(1-q_T)/2$.

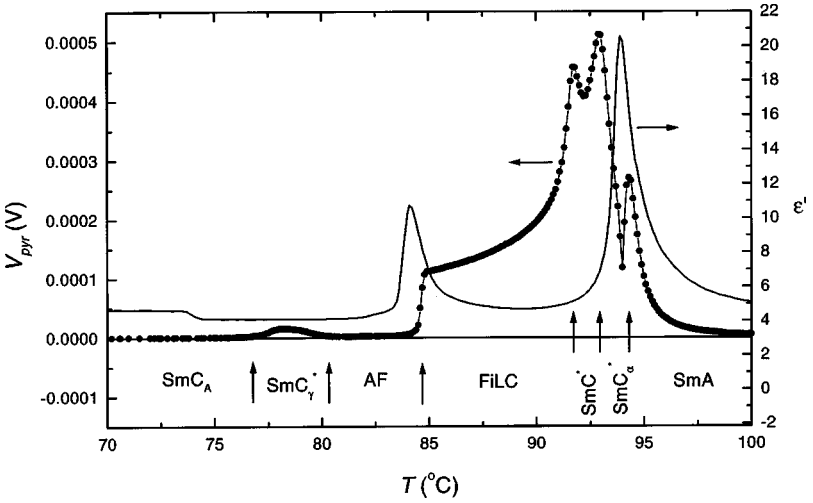

FIG. 2. Temperature dependencies of pyroelectric response V_{pyr} and dielectric permittivity ε' for bias electric fields 0.15 and 1.1 V/μm, respectively.

We represent the spontaneous polarization of the ith phase with an external field E_{dc} as $P_i = r_i(E_{\mathrm{dc}})P_S$, where the phenomenological coefficient $r_i(E_{\mathrm{dc}})$ describes a phase with an external field E_{dc}. The macroscopic polarization in the sample is evaluated by summing the projections of dipole moments from all smectic layers over a period of the helix:

$$\overline{P}(T,E_{\mathrm{dc}}) = \frac{1}{Z}\int_0^Z P_i \cos\phi(z)\,dz = r_i(E_{\mathrm{dc}})P_S\,\overline{\cos\phi}, \tag{10}$$

where the azimuthal angle ϕ is the angle between the polarization of the smectic layer and the X axis. Now the intrinsic pyroelectric coefficient can be expressed as follows:

$$\gamma(T,E_{\mathrm{dc}}) = \frac{d\overline{P}(T,E_{\mathrm{dc}})}{dT} = r_i(E_{\mathrm{dc}})\left(\frac{dP_S}{dT}\,\overline{\cos\phi} + P_S\frac{d\,\overline{\cos\phi}}{dT}\right). \tag{11}$$

The total pyroelectric coefficient γ_T is represented as

$$\gamma_T(T,E_{\mathrm{dc}}) = \varepsilon_0\frac{d\overline{\varepsilon}}{dT}E_{\mathrm{dc}} + r_i(E_{\mathrm{dc}})\left(\frac{dP_S}{dT}\,\overline{\cos\phi} + P_S\frac{d\,\overline{\cos\phi}}{dT}\right). \tag{12}$$

The pyroelectric coefficient increases with the bias field until a critical electric field is reached when the pitch of the helix goes to infinity and the structure of the phase is unwound. For bias fields greater than the threshold for a complete helical unwinding, $\overline{\cos\phi}$ is constant and is equal to its maximal value of 1; the temperature derivative of $\overline{\cos\phi}$ is equal to zero. The first term in Eq. (12) also has a minimal value for such fields, if the temperature is not too close to the Sm$A^*\rightarrow$SmC^* phase transition, and can be neglected in comparison to the second term. In this case Eq. (12) can be simplified to the form

$$\gamma_T(T,E_{\mathrm{dc}}) = r_i(E_{\mathrm{dc}})\,\gamma_S(T), \tag{13}$$

where $\gamma_S(T)$ is the pyroelectric coefficient of ferroelectric SmC^* phase. Since we are not interested in the absolute values of the pyroelectric coefficients, but only in their dependence on temperature or bias field in different phases, the coefficient $r_i(E_{\mathrm{dc}})$ is calculated directly from the experimental results as the normalized pyroelectric response

$$r_i(E_{\mathrm{dc}}) = \frac{V_{\mathrm{pyr}}(T,E_{\mathrm{dc}})}{V_S(T)}, \tag{14}$$

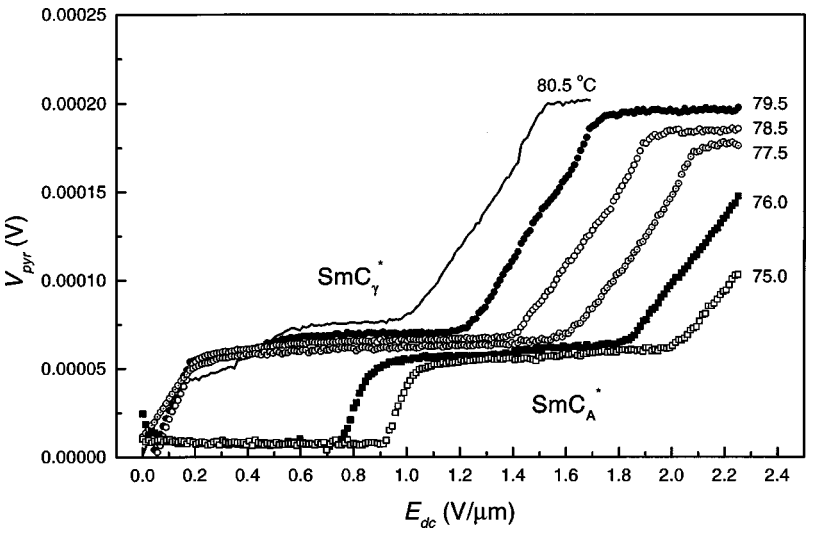

FIG. 3. Dependencies of pyroelectric response on a bias field in SmC_A^* and SmC_γ^* phases for several temperatures.

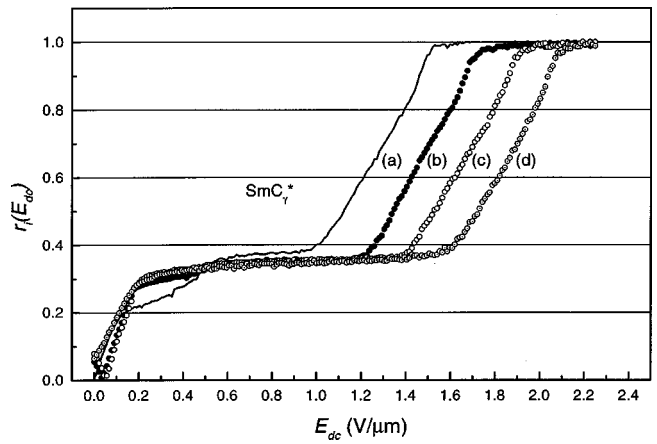

FIG. 4. Dependencies of coefficient $r_i(E_{\rm dc})$ on a bias field in SmC_γ^* phase for several temperatures: 80.5 °C (a), 79.5 °C (b), 78.5 °C (c), and 77.5 °C (d).

where $V_S(T)$ is the pyroelectric response for the field-induced SmC^* phase at temperature T. This is possible because a pyroelectric voltage measured by lock-in amplifier is proportional to the pyroelectric coefficient: $V_{\rm pyr} = R_L A(dT/dt)\gamma_T$; here R_L is the input resistance of the measuring scheme. Coefficient $r_i(E_{\rm dc})$ calculated using Eq. (14) coincides with that defined by Eq. (13) for structures with unwound helices.

As was mentioned before, $r_i(E_{\rm dc})$ corresponds to the ratio $1/n$ (characterizing the spontaneous polarization of the AFLC phase in the one dimensional Ising model [8]) for bias fields when the helical structure is unwound and $r_i(E_{\rm dc})$ becomes approximately constant. In this case it can be used to characterising the field-induced AFLC phases. An increase in the coefficient $r_i(E_{\rm dc})$ to a new stable level with an increase in the bias field indicates a field-induced phase transition from one phase to the next.

IV. RESULTS AND DISCUSSION

Figure 2 presents the dependence of the pyroelectric response on temperature when the bias field is lower than the critical field for helical unwinding in the SmC^* phase. According to this plot the pyroelectric signal is present in the SmC_α^* phase, the ferroelectric SmC^* phase, the ferrielectric SmC_γ^* phase and the FiLC phase. The pyroelectric signal in these phases appears to be due to a distortion of the helical structures arising from the interaction of the spontaneous polarization with the bias electric field. In the antiferroelectric AF and SmC_A^* phase, the pyroelectric response is absent because the spontaneous polarization in both these phases is equal to zero.

The effect of bias field on the pyroelectric signal in the SmC_A^* and SmC_γ^* phases is given in Fig. 3. At temperatures of 75 and 76 °C, which correspond to the antiferroelectric SmC_A^* phase, the pyroelectric response is low, and independent of bias field until 1.0 and 0.85 V/μm, respectively, where the field-induced phase transition to the ferrielectric SmC_γ^* phase is reached. The field-induced transition to the unwound SmC^* structure starts for these temperatures at fields of 2.0 and 1.85 V/μm, respectively. It is important to note that the SmC_γ^* phase is unwound just after the phase transition from the SmC_A^* phase; otherwise the pyroelectric response would be almost zero. This finding is similar to that of Hiraoka *et al.* [21] from conoscopy measurements.

The field dependencies of the pyroelectric response corresponding to several temperatures in the SmC_γ^* phase (Fig. 3) show a typical ferrielectric dependence on bias field both for the spontaneous polarization [15] and for the apparent tilt angle [22]. In the ferrielectric SmC_γ^* phase the pyroelectric response increases considerably with the bias field, due to a helical unwinding process which starts from a very low value of the bias field. A linear increase of the signal with the bias field is observed during the field-induced transition Sm$C_\gamma^* \rightarrow$ SmC^*. This is valid for all temperatures in the SmC_γ^* phase. The threshold field of the field-induced phase transition from SmC_γ^* to SmC^* phases decreases with an increase in temperature. Figure 4 shows the field dependence of the normalized pyroelectric response in terms of the phenomenological coefficient $r_i(E_{\rm dc})$ for the same temperatures as in the SmC_γ^* phase. As expected, for bias fields greater than the critical field of the ferrielectric helix unwinding, $r_i(E_{\rm dc})$ is equal to the ratio $1/n$ of the one-

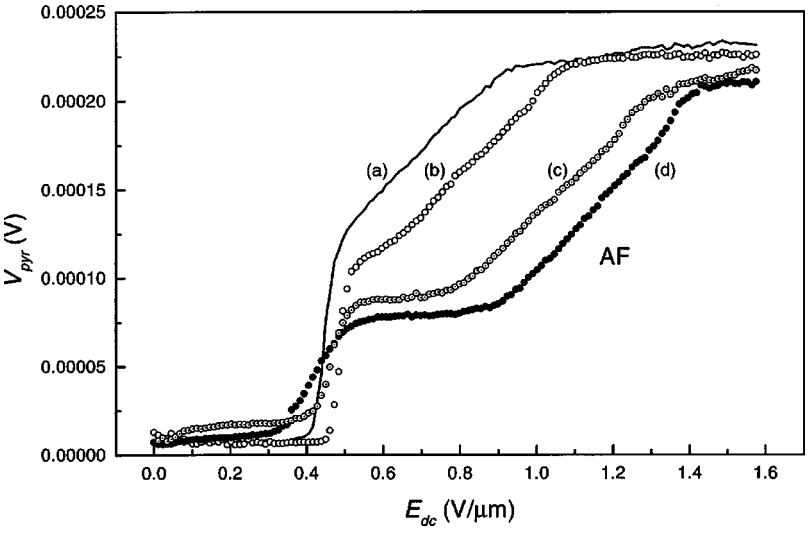

FIG. 5. Pyroelectric response as a function of bias field in the antiferroelectric AF phase at various temperatures: 83.0 °C (a), 82.5 °C (b), 81.5 °C (c), and 81.0 °C (d).

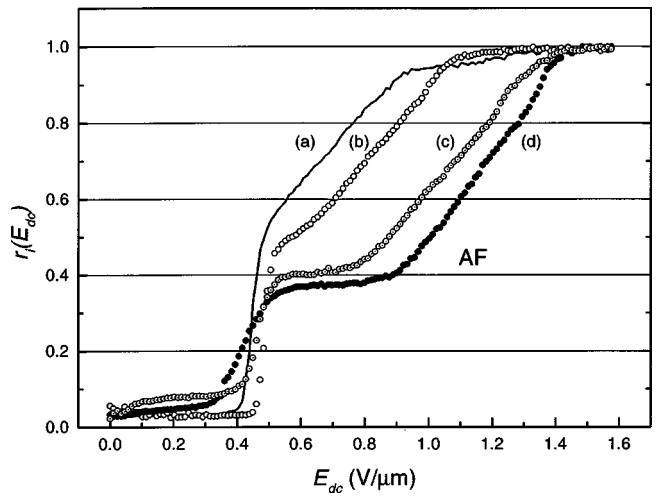

FIG. 6. Coefficient $r_i(E_{\mathrm{dc}})$ as a function of bias field in the antiferroelectric AF phase at various temperatures: 83.0 °C (a), 82.5 °C (b), 81.5 °C (c), 81.0 °C (d).

dimensional Ising model [8] for the SmC^*_γ phase, and is $\sim\frac{1}{3}$ for all temperatures.

The dependence of the pyroelectric signal and the coefficient $r_i(E_{\mathrm{dc}})$ on the bias field in the low temperature region (Figs. 5 and 6, curves 81.0 °C and 81.5 °C) looks similar to that in the SmC^*_A phase. The phase in this temperature range is designated as AF. One observes a low signal until the field-induced phase transition to the ferrielectric SmC^*_γ phase is reached; then the signal reaches a plateau corresponding to the unwound SmC^*_γ phase, after which a field-induced transition to the ferroelectric SmC^* phase occurs. In this high temperature region, the field-induced transition from the antiferroelectric AF phase goes directly to the ferroelectric SmC^* phase, without going through the SmC^*_γ phase. This experimental result, i.e., a kind of dependence of the field-induced phase transitions on the temperature region of the AF phase, partly confirms the theoretical prediction of Yamashita and Tanaka [12] (Fig. 1). However, a divergence exists between theory and our experimental results, namely, experimental data do not confirm the existence of the ferrielectric phase with $q_T=3/7(q=2/7)$, which should precede the SmC^*_γ phase, with the field increasing in low temperature region. Instead of the three field-induced phase transitions predicted by theory, namely, $q_T=1/2(\mathrm{AF})\rightarrow q_T=\frac{3}{7}$, $q_T=\frac{3}{7}\rightarrow q_T=\frac{1}{3}(\mathrm{Sm}C^*_\gamma)$, and $q_T=\frac{1}{3}(\mathrm{Sm}C^*_\gamma)\rightarrow q_T=1(\mathrm{Sm}C^*)$, experimentally only two transitions are observed: $q_T=\frac{1}{2}(\mathrm{AF})\rightarrow q_T=\frac{1}{3}(\mathrm{Sm}C^*_\gamma)$ and $q_T=\frac{1}{3}(\mathrm{Sm}C^*_\gamma)\rightarrow q_T=1(\mathrm{Sm}C^*)$. It is worth noting that $r_i(E_{\mathrm{dc}})$ for the field-induced ferrielectric phase in the low temperature region of the AF phase is somewhat higher than $\frac{1}{3}$ for the SmC^*_γ phase.

The dependence of the pyroelectric signal on the bias field for the SmC^* phase is shown in Fig. 7 (93.0 and 92.5 °C). An initial linear response of the signal with the bias field, corresponding to the helix distortion, is followed by a dependence with a lower slope when the bias field approaches the critical field for the helix unwinding. From these curves we find that the critical field for a helical unwinding in the ferroelectric SmC^* phase is ~0.5 V/μm. A decrease in the pyroelectric response with a further increase in field can be explained by the first term of Eq. (12). This term has sign opposite to that of the intrinsic pyroelectric coefficient for temperatures below the Sm$A^*\rightarrow$SmC^* phase transition, because for these temperatures the soft mode contribution to the dielectric permittivity decreases with temperature. In Fig. 7 the pyroelectric signal for the FiLC phase at 92.0 °C is also presented. Two slopes for an increase in signal separated by a saturation region are observed in this case. The slope at higher fields is connected with an unwinding of the ferroelectric helical structure. This assignment follows from a comparison with the field dependence of the pyroelectric signal for the SmC^* phase. In addition to the process of the ferroelectric structure unwinding another process appears in this phase for bias fields less than 0.2 V/μm, and leads to a stable structure which is different from the unwound SmC^* phase.

Figure 8 demonstrates the dependence of the pyroelectric response on the bias field for several temperatures in the FiLC phase. The common feature of the dependence of the signal on the field for all temperatures is that two regions of steep signal increases are separated by a region of a slow change in the signal. The high field increase corresponds to an unwinding of the ferroelectric structure. This shifts to higher fields with a decrease in temperature. The low field slope starts from the bias fields almost greater than zero field; $r_i(E_{\mathrm{dc}})$ depends on the bias field (Fig. 9) and on the

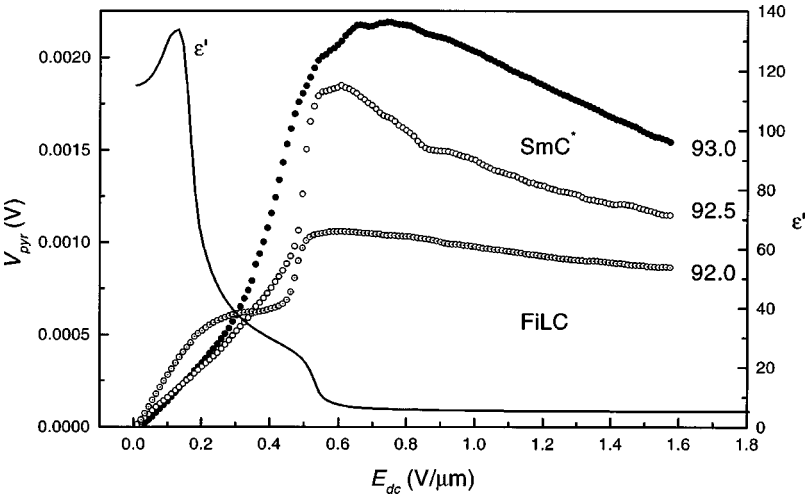

FIG. 7. Dependence of the pyroelectric signal on the bias field in SmC^* (93 and 92.5 °C) and in FiLC phase (92 °C). Dielectric permittivity ε' as a function of bias field in FiLC phase (92 °C).

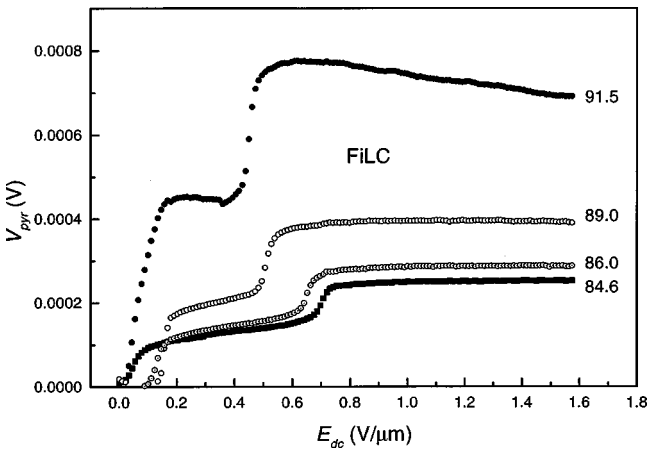

FIG. 8. Pyroelectric response as a function of bias field in the ferroelectric FiLC phase at various temperatures.

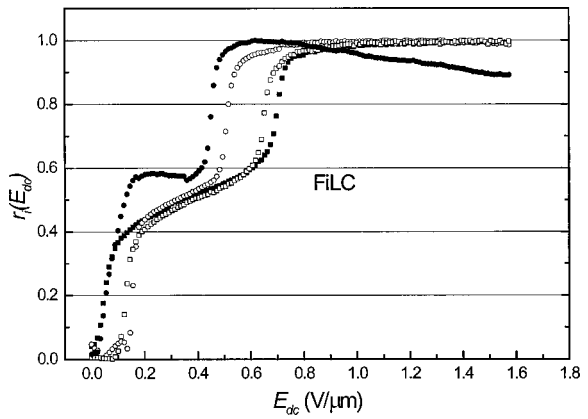

FIG. 9. Coefficient $r_i(E_{\mathrm{dc}})$ as a function of the bias field in the ferrielectric FiLC phase at various temperatures: 91.5 °C (●), 89.0 °C (○), 86.0 °C (□), and 84.6 °C (■).

temperature within the FiLC phase. A stable value of $r_i(E_{\mathrm{dc}}) \approx 0.6$ is observed only in the high temperature region of the FiLC phase. For lower temperatures it depends on the bias field, and changes from 0.4 to 0.6 approximately linearly with the field.

In order to explain the unusual behavior of the pyroelectric response observed in this phase, dielectric measurements and the texture with a polarising microscopy were also observed. In Fig. 7 the results of the dependence of the dielectric permittivity ε' on the bias field at a temperature of 92 °C are also presented. The latter shows that, in addition to the ferroelectric Goldstone mode being suppressed at a bias field of 0.5 V/μm, another process is suppressed at even lower fields (<0.2 V/μm). The mechanism of this process of suppression is not clear yet. It was reported [15] that the dielectric spectrum of the 12OF1M7 (previously called AS-573) possesses two relaxation processes in this temperature region: one is the ferroelectric Goldstone mode; and another can be assigned to the ferrielectric Goldstone mode because it also exists in the ferrielectric SmC^*_γ phase.

Textures of the FiLC phase under the bias field were observed using a polarizing microscope. At temperatures of 89 and 86 °C an increase of the bias field up to 0.15 V/μm leads to the appearance of the first domain texture. The sharp black-white stripes with a period of several microns are oriented perpendicularly to the rubbing direction, and thus parallel to the smectic layers. A further increase in the bias field results in a disappearance of the domain texture. But when the field reaches values of 0.5 V/μm at 89 °C and 0.65 V/μm at 86 °C (see Fig. 8), the second domain texture is observed. The orientation of the second domain system is similar to the first one, but the stripes are more smooth, and their period is longer than that of the first system. The appearance of the domain textures in this phase seems to be a result of an unwinding of a helical structure in the two stages. One notes that the bias fields, for which the domain textures appear, coincide with the regions of an increase in the pyroelectric signal (Fig. 8).

The pyroelectric results are found to agree with the dielectric and polarization measurements [15]. The dependencies of the pyroelectric signal on the bias field show interesting behavior for SmC^*_A, SmC^*_γ, AF, and SmC^* phases. For the FiLC phase, both the pyroelectric response and the dielectric permittivity under the bias field exhibit interesting and unusual features. The ANNNI model with third-nearest-neighbor interaction [23] in this temperature region predicts the existence of one commensurate phase and two incommensurate phases with wave numbers q, correspondingly, of $\frac{1}{5}(q_T=\frac{3}{5})$, $\frac{3}{14}(q_T=\frac{4}{7})$, and $\frac{2}{9}(q_T=\frac{5}{9})$.

The Landau model [6], involving an expansion of free energy in terms of ferroelectric and antiferroelectric order parameters, predicts that transitions from the SmC^* phase to other phases go through incommensurate or soliton-lattice type phases in some cases. These phases represent a structure of the domain walls on a helix. Hence one can expect that two dielectric relaxation processes coexist for these phases: a Goldstone mode of a helix, and a mode involving a soliton-lattice motion. The soliton in this model is a domain wall that lies essentially in between two commensurate regions. The soliton-lattice state is formed by including a domain wall every few periods of a helix. As a consequence, the period of the soliton lattice is probably longer than the pitch of a helix in the commensurate regions. In general, the macroscopic polarization of the deformed helical structure of the domain wall is compensated for by the polarization of the other domain walls. When an electric field is applied across the cell in this incommensurate phase, an unwinding of the soliton-lattice occurs first, accompanied by the alignment of the macroscopic polarization of the domain wall along the direction of the field. The threshold field of this process is much lower than for helical unwinding in commensurate regions, for the reason that the threshold field is inversely proportional to the period of the helix. This corresponds to a first stepwise increase in the pyroelectric response with field. The second stepwise increase corresponds to the helical unwinding in the commensurate regions and a transition to an unwound SmC^* phase. The observation of the phase transition from FiLC to AF phases, depending on the temperature within the FiLC phase, is also due the existence of an incommensurate type phase. In Fig. 2 the temperature dependence of the dielectric permittivity ε' is presented, with the bias field of 1.1 V/μm applied across the sample. One can seethat the Goldstone mode in FiLC phase is suppressed by this field, and the peak in the relative permittivity that is observed is due to the soliton-lattice mode, coinciding with the FiLC→AF phase transition. Thus the FiLC phase seems to

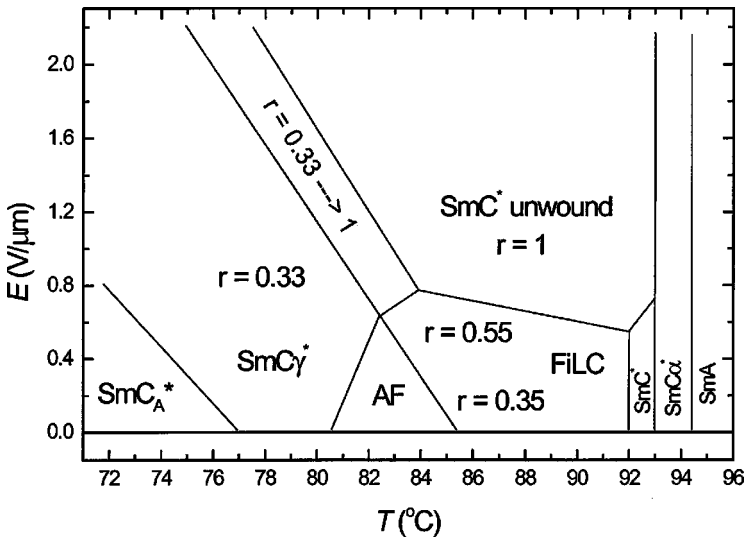

FIG. 10. *E-T* phase diagram of 12OF1M7 determined by the pyroelectric measurements.

be one of the incommensurate phases, predicted by the ANNNI and Landau models [23,6], for the temperature region between the ferroelectric SmC^* phase and the antiferroelectric AF phase, and that many of the unusual features of this phase find their explanations in terms of these models.

V. CONCLUSIONS

Pyroelectric measurements confirm the existence of several antiferroelectric and ferrielectric phases in an antiferroelectric liquid crystal, with a phase sequence of SmC_A^*-SmC_γ^*-AF-FiLC-SmC^*-SmC_α^*, in the absence of an external field.

In the antiferroelectric SmC_A^* phase, the threshold field of the field-induced transition from SmC_A^* to SmC_γ^* phases depends on a temperature: the higher the temperature, the lower the threshold field. The field-induced transition from SmC_A^* to SmC_γ^* phases is sharp; that is, the range from a threshold field to a saturation field is less than 0.2 V/μm. It is found that the SmC_γ^* phase is unwound just after a phase transition from SmC_A^* to SmC_γ^* phases.

The threshold field of the field-induced transition from SmC_γ^* to SmC^* phases, observed in SmC_A^*, SmC_γ^*, and AF phases, decreases monotonically with an increase in temperature. The field-induced transition from SmC_γ^* to SmC^* phases is more than two times wider than the field-induced transition from SmC_A^* to SmC_γ^* phases and has a range, from the beginning of the transition to the end, of approximately 0.5 V/μm. In the SmC_γ^* phase a helical structure is unwound with a weak field of $\sim$ 0.2 V/μm.

In the low-temperature region, the AF phase shows a field-induced transition to the SmC_γ^* phase, with a field of almost 0.5 V/μm, and the SmC_γ^* phase is unwound just after the phase transition from the AF phase. The wideness of this field-induced transition is the same as for transition from SmC_A^* to SmC_γ^* phases. In the high temperature region of the AF phase, our results show a field-induced transition directly from AF to SmC^* phases without going through an intermediate SmC_γ^* phase. The field-induced phase transitions determined from these experiments are summarized in Fig. 10.

The pyroelectric data confirm the main theoretical predictions of the ANNNI model (Yamashita and Tanaka [12]) for the basic phases of SmC_A^*, SmC_γ^*, AF, and SmC^* phases. In particular, it was found that the type of field induced phase transition from the AF phase differs for low and high temperatures for a range of temperatures of the AF phase.

The pyroelectric and dielectric results of the FiLC phase show the difference between FiLC phase and a typical SmC^* phase. The FiLC phase seems to be one of the incommensurate phases, predicted for the temperature region between SmC^* and AF phases, both by the ANNNI and Landau models.

ACKNOWLEDGMENTS

This work was supported by European ORCHIS network, and partly by RFBR Grant No. 98-02-17071.

[1] A. Fukuda, Y. Takanishi, T. Isozaki, K. Ishikawa, and H. Takezoe, J. Mater. Chem. **4**, 997 (1994).
[2] M. Fukui, H. Orihara, Y. Yamada, N. Yamamoto, and Y. Ishibashi, Jpn. J. Appl. Phys. **28**, L849 (1989).
[3] T. Sako, Y. Kimura, R. Hayakawa, N. Okabe, and Y. Suzuki, Jpn. J. Appl. Phys. **35**, L114 (1996).
[4] P. Mach, R. Pindak, A.-M. Levelut, P. Barois, H. T. Nguyen, C. C. Huang, and L. Furenlid, Phys. Rev. Lett. **81**, 1015 (1998).
[5] H. Orihara and Y. Ishibashi, Jpn. J. Appl. Phys. **29**, L115 (1990).
[6] B. Zeks and M. Cepic, Liq. Cryst. **14**, 445 (1993).
[7] V. L. Lorman, A. A. Bulbitch, and P. Toledano, Phys. Rev. E **49**, 1367 (1994).
[8] T. Isozaki, K. Hiraoka, Y. Takanishi, H. Takezoe, A. Fukuda, Y. Suzuki, and I. Kawamura, Liq. Cryst. **12**, 59 (1992).
[9] P. Bak and R. Bruinsma, Phys. Rev. Lett. **49**, 249 (1982).
[10] Y. Yamada and N. Hamaya, J. Phys. Soc. Jpn. **52**, 3466

(1983).
[11] M. Yamashita and S. Miyazima, Ferroelectrics **148**, 1 (1993).
[12] M. Yamashita and S. Tanaka, Jpn. J. Appl. Phys. **37**, L528 (1998).
[13] S. Pikin, M. Gorkunov, D. Kilian, and W. Haase, Liq. Cryst. **26**, 1107 (1999).
[14] A. Kocot, R. Wrzalik, J. K. Vij, and R. Zentel, J. Appl. Phys. **75**, 728 (1994); J. W. O'Sullivan, Yu. P. Panarin, and J. K. Vij, *ibid.* **77**, 1201 (1995).
[15] Yu. P. Panarin, O. Kalinovskaya, J. K. Vij, and J. W. Goodby, Phys. Rev. E **55**, 4345 (1997).
[16] J. W. O'Sullivan, Yu. P. Panarin, J. K. Vij, A. J. Seed, M. Hird, and J. W. Goodby, J. Phys.: Condens. Matter **8**, L551 (1996).
[17] N. M. Shtykov, J. K. Vij, V. P. Panov, R. A. Lewis, M. Hird, and J. W. Goodby, J. Mater. Chem. **9**, 1383 (1999).
[18] A. M. Glass, J. S. Patel, J. W. Goodby, and D. H. Olson, J. Appl. Phys. **60**, 2778 (1986).
[19] A. G. Chynoweth, J. Appl. Phys. **27**, 78 (1956).
[20] L. A. Beresnev and L. M. Blinov, Ferroelectrics **33**, 129 (1981).
[21] K. Hiraoka, A. D. Chandani, E. Gorecka, Y. Ouchi, H. Takezoe, and A. Fukuda, Jpn. J. Appl. Phys. **29**, L1473 (1990).
[22] K. Hiraoka, Y. Takanishi, K. Skarp, H. Takezoe, and A. Fukuda, Jpn. J. Appl. Phys. **30**, L1819 (1991).
[23] M. Yamashita, Mol. Cryst. Liq. Cryst. **303**, 153 (1997).